RSC Advances

ROYAL SOCIETY OF CHEMISTRY

www.rsc.org/advances

Cite this: DOI: 10.1039/c0xx00000x

www.rsc.org/xxxxxx

ARTICLE TYPE

Facile synthesis of WO_3 with reduced particle size on Zeolite-Y and enhanced photocatalytic activity

S. Prabhu,[a] K. Jothivenkatachalam,[a *] and K. Jeganathan[b]

Received (in XXX, XXX) Xth XXXXXXXXX 20XX, Accepted Xth XXXXXXXXX 20XX

DOI: 10.1039/b000000x

WO_3 supported on Zeolite-Y **(WO_3-ZY)** was successfully synthesized by the facile impregnation method and well characterized by various techniques. The photocatalytic activity of the prepared catalysts was investigated for the degradation of Rhodamine B (RhB) under visible, UV and solar light irradiation. The enhanced photocatalytic activity was observed by the catalyst **WO_3-ZY** which may be due to the presence of more active sites to adsorb more number of dye molecules. The TEM, FESEM and adsorption studies confirm that the WO_3 supported on Zeolite-Y have a very small particle size of about 8 nm compared to the bare WO_3 of 97 nm. The efficient electron-hole pair separation and the role of active species were investigated by PL spectroscopy and the effect of scavengers test respectively. The mechanism for the photocatalytic degradation of RhB was proposed and the pathway of RhB degradation was illustrated schematically.

Introduction

Semiconductor photocatalysis is a promising technique to address the environmental issues such as energy storage and decontamination of environmental pollution.[1] This technique provides clean and recyclable hydrogen energy and also it can utilize solar energy to decompose organic and inorganic pollutants present in air and aqueous media.[2, 3] It is well known that TiO_2 is the most widely used best photocatalytic material. However, only a small fraction of solar light (3-5 %) can be utilized due to its wide band gap.[4,5] Even though the visible light photocatalytic activity of TiO_2 has been reported in nitrogen-doped TiO_2, the quantum efficiency of the nitrogen-doped TiO_2 is much lower than that under UV light irradiation.[6] In contrast, WO_3 is n-type semiconductor which has strong absorption in solar spectrum, stable physicochemical properties, and resistant to photocorrosion effects.[7] The narrow band gap of about 2.4-2.8 eV and deeper valance band (+3.1 eV) has gained additional advantages for visible light driven photocatalysis.[7] However, due to fast recombination of electron-hole pair and low conduction band level, pure WO_3 is not an efficient photocatalyst.[8] The photocatalytic efficiency of the pure WO_3 can be enhanced by several methods. Some of them are tuning the physical property such as morphology and particle size,[9-12] semiconductor coupling,[13-16] nobel metal deposition,[7, 14, 15, 17] metal ion doping,[18] etc. Increasing the surface area and suppressing the electron-hole pair recombination can enhance the photocatalytic activity of WO_3.[8] There are very limited reports available on tuning the physical properties of WO_3 to improve the efficiency under visible light irradiation.[19]

In Recent, the researchers have intensively focused on mesoporous materials such as zeolite, as a support for metal oxides which influence the photocatalytic activity through structural modification.[20- 23] The Zeolitic materials have gained significant importance due to its high surface area, thermal stability and specific photophysical properties on charge and electron transfer processes.[24, 25] The use of zeolite, as a support for metal oxides improves the amount of photons absorbed by the catalyst and reduces the amount of metal oxides required.[26] Despite, there are several metal oxides were supported on zeolitic materials and proven to be a better photocatalyst, there is no report on WO_3 supported on zeolitic materials for photocatalytic applications.

For the first time, we report the facile synthesis of WO_3 supported on Zeolite-Y catalyst by impregnation method and its photocatalytic efficiency for the degradation of RhB under visible, UV and solar light irradiation. The prepared catalysts were well characterized by Powder X-ray diffraction (PXRD), X-ray photoelectron spectroscopy (XPS), Transmission electron microscopy (TEM), Field Emission scanning electron microscope (FESEM), Raman, Fourier transform infrared spectroscopy (FT-IR) and UV-vis Diffuse reflectance spectra (UV-DRS) techniques. The highly enhanced photocatalytic activity was observed by the catalyst WO_3 loaded on Zeolite-Y. The TEM, FESEM and adsorption study confirms reduced particle size of the catalyst. The efficient electron-hole pair separation of the catalysts was investigated by PL spectroscopic techniques. The photocatalytic activity in the presence of different scavengers was demonstrated to testing which active species plays an important role in the degradation of the RhB. The mechanism for the photocatalytic degradation of RhB was proposed and the pathway of RhB degradation was also illustrated schematically.

Experimental

Materials

All analytical grade reagents of $Na_2WO_4.2H_2O$, H_2WO_4, RhB, $BaSO_4$ and Zeolite-Y were used as such without further purification. Deionized and double distilled water was used throughout this work.

Synthesis

The WO_3 supported Zeolite-Y **(WO_3-ZY)** catalyst was prepared by the facile impregnation method as follows. The Zeolite-Y of 1 g was taken in aqueous medium and stirred. After that 5 g of H_2WO_4 was added into the above reaction mixture. Then, the reaction mixture was refluxed at 100 ˚C for 24 hrs. The obtained precipitate was collected by centrifugation, washed several times using distilled water and dried. The dried sample was calcinated at 500 ˚C for 3 hrs. For comparison, pure WO_3 was prepared by the precipitation method as reported in the literature. [27] The sodium tungstate was dissolved in distilled water and heated up to 85 ˚C slowly. The appropriate amount of a warm, concentrated nitric acid was added drop wise to this solution with vigorous stirring. The mixed solution was kept at the same temperature for 30 min under continuous stirring. The precipitate was allowed to settle for overnight at room temperature. The precipitate was washed by the addition of a large amount of water and allowing the precipitates to settle down before decanting the liquid. Finally, the precipitate was separated by centrifugation and dried. After drying, the pure **WO_3** was calcined at 500 ˚C for 3 hrs.

Characterization

PXRD data collected from PAN analytical X'pert Pro dual goniometer diffractometer. The data were collected with a step size of 0.008°and a scan rate of 0.5° min^{-1}. The radiation used was Cu-Kα (1.5418 Å) with Ni filter and the data collection was carried out using a flat holder in Bragg–Brentango geometry. XPS analysis was carried out by Kratos Axis-Ultra DLD instrument by passing 200 eV energy. During XPS analysis the sample was irradiated with Mg Kα and the data collected by sweep rate of 2 eV and 5 eV in a wide and narrow range scan respectively. TEM analysis was done by JEOL model 2010 FasTEM instrument with accelerating voltage of 200 kV. FESEM image was obtained from Carl Zeiss ∑IGMA instrument with the resolution of 1.2 nm. The Energy dispersive X-ray spectra (EDX) were recorded using INCAx-act Oxford Instrument equipped with SEM. Raman spectra were recorded by employing Horiba JY LabRAMHR 800 Raman spectrometer coupled with microscope in reflectance mode with 514 nm excitation laser source. UV-DRS spectra were recorded on Shimadzu UV-2450 UV–Visible Spectrophotometer equipped with an integrated sphere assembly using $BaSO_4$ as a reflectance sample. FT-IR analysis was performed using Jasco FT-IR 460 plus spectrophotometer. The PL spectrum was recorded by JASCO FP-6500 Spectrofluorimeter with excitation wavelength of 300 nm.

Photocatalytic test

The photocatalytic degradation of a model pollutant RhB was chosen to investigate the photocatalytic activity of the prepared catalysts. In a typical experiment, 25 mg of the catalyst was suspended in 50 ml of aqueous solution contains 10 mg/L of RhB dye. Prior to irradiation, the suspension was kept to attain adsorption-desorption equilibrium by aeration for 30 min in the dark. The photocatalytic activity was investigated under visible and UV light irradiation by 300W Tungsten Halogen lamp (8500 lumen) and 125 W medium pressure mercury lamp emitting 365 nm (110 μW cm^{-2}, measured by Lutron UV light Meter) light respectively. The reaction mixture was aerated continuously while irradiation, to through mixing of the reaction mixture. At the given time interval 3.5 ml of the sample was withdrawn and centrifuged to separate the catalyst. The degradation of RhB was determined by measuring the maximum absorbance at 554 nm on UV–Visible Spectrophotometer.

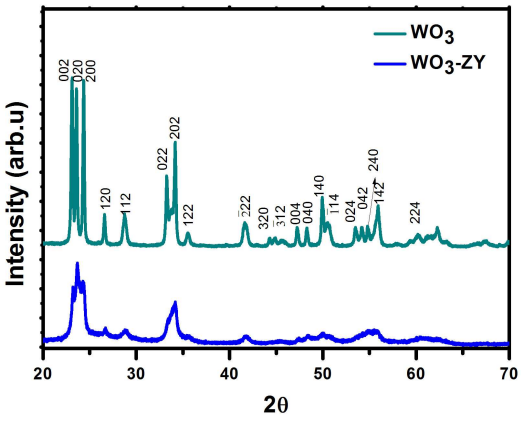

Fig. 1 PXRD pattern of the **WO_3** and **WO_3-ZY**.

Results and discussion

Characterization

Crystalline structure

PXRD pattern of the prepared catalysts is shown in Fig. 1. The peaks obtained in the pattern are indexed with standard data (JCPDS no. 83-0950) and corresponds to the monoclinic phase structure. In pure **WO_3**, the pattern shows very sharp peaks which represent the high crystalline and of the greater in particle size. The diffraction peaks appeared in the **WO_3-ZY** corresponds to WO_3 indicating the formation of WO_3 on the Zeolite-Y. Please see the supporting information for the PXRD pattern of pure Zeolite-Y. On the other hand, there are no sharp peaks in the diffraction pattern of **WO_3-ZY** which attributed the smaller size particles of WO_3. The crystalline size of the **WO_3** and **WO_3-ZY** in (002) plane is calculated by Scherer formula and it is around 43 and 26 nm respectively. This result shows that the growth of **WO_3** on Zeolite-Y is very limited and controlled.

Morphology and particle size

The FESEM image of the **WO_3** sample shows spherical shaped particles with the average size of 102 nm as shown in Fig. 2(a). The FESEM image of **WO_3-ZY** shows very small particles (12 nm) as shown in Fig. 2(c). Since there are no distinct particles, it is difficult to obtain particle size from the image. For comparison, the FESEM image of Zeolite-Y is shown in Fig. 2(b) The TEM image of **WO_3** is given in Fig. 2(d) which further confirms the shape of the particles. The average particle size calculated from the TEM image to be around 97 nm which is close to the one calculated from FESEM image. The high magnified TEM image of **WO_3** is shown in Fig. 2(e). The inter-planar distance from the

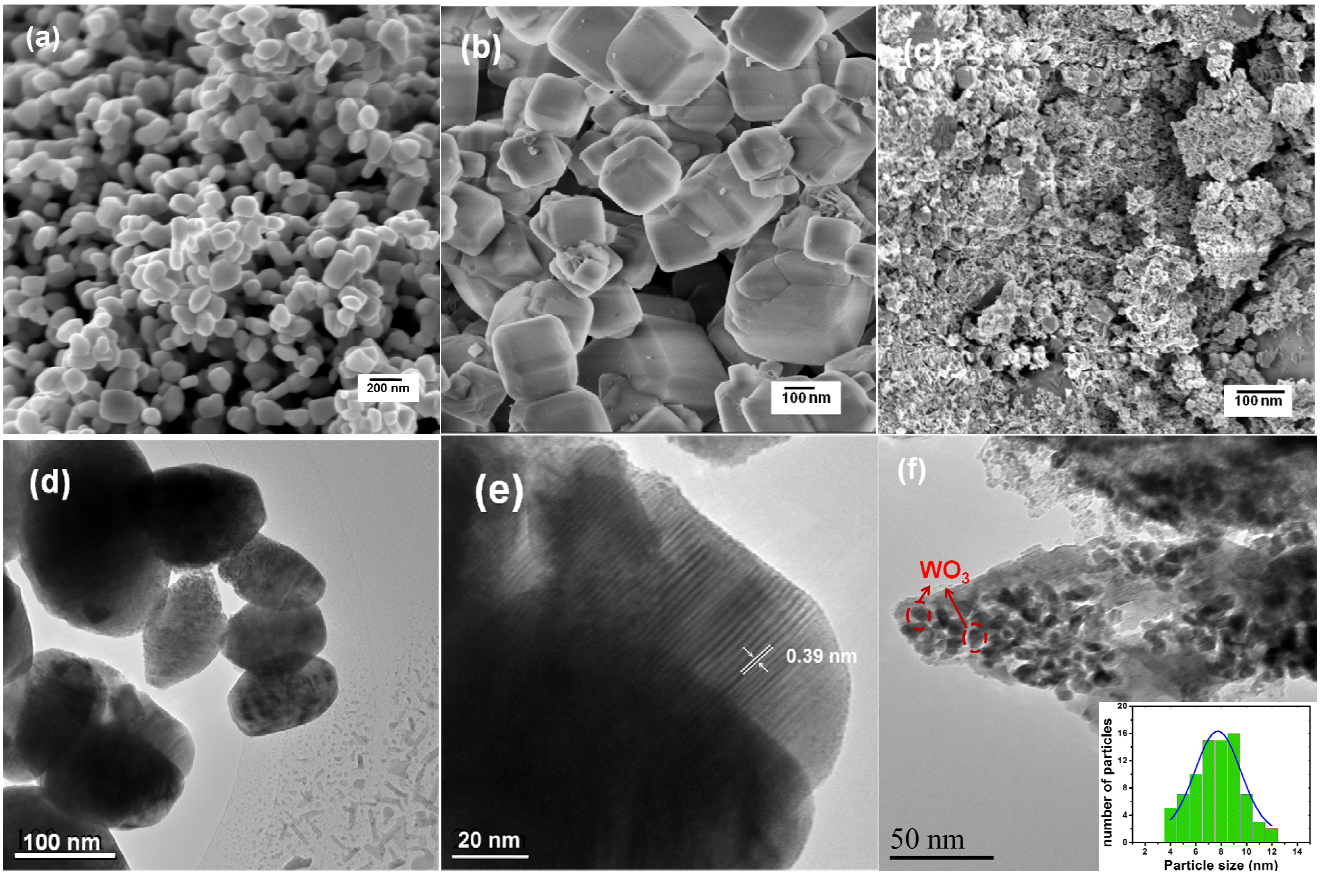

Fig.2 FESEM image of (a). **WO_3,** (b). Zeolite-Y, (c). **WO_3-ZY**, (d, e) TEM and HR TEM image of **WO_3** and (f) TEM image of **WO_3-ZY.**

TEM image was calculated to be 0.39 nm, which is well matched with the lattice spacing of (200) planes of the monoclinic WO_3 structure. The TEM image of **WO_3-ZY** shows that, the particles are in very small size as shown in Fig. 2(f) and the particle size distribution shown in insert figure. The calculated average particle size of **WO_3-ZY** from Fig. 2(f) is to be around 8 nm. This FESEM and TEM results shows that, the WO_3 particle size was reduced from 97 nm to 8 nm at the given reaction condition. This decrease in particle size may provide more active sites. The elements present in the catalysts **WO_3** and **WO_3-ZY** were confirmed by the EDX analysis and are shown in Fig. 3(a, b).

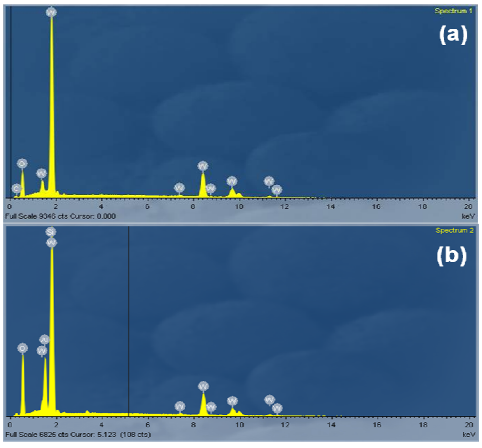

Fig. 3 EDX spectrum of (a). **WO_3**, (b). **WO_3-ZY**.

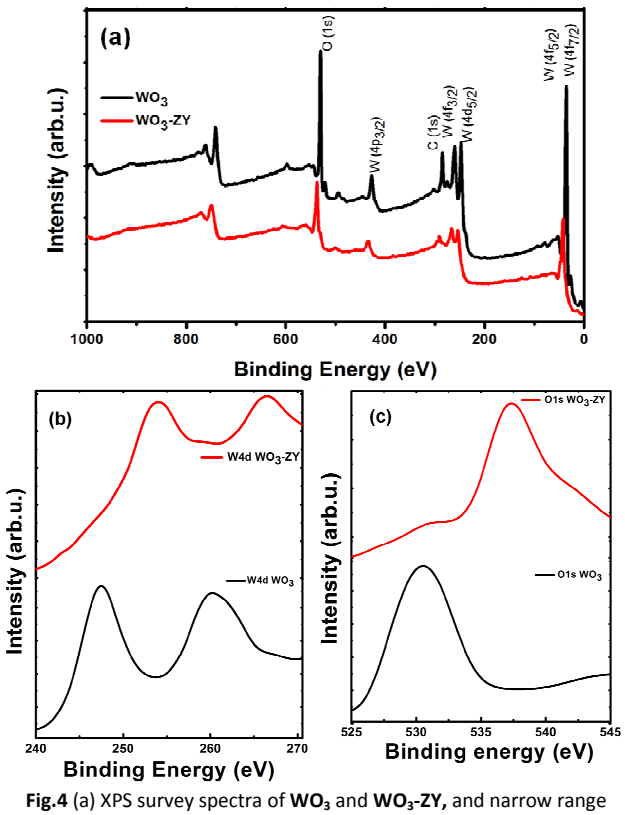

Fig.4 (a) XPS survey spectra of **WO_3** and **WO_3-ZY,** and narrow range survey spectra of (b) W4d, (c) O1s of **WO_3** and **WO_3-ZY**.

XPS analysis

The elements and its chemical states present in the catalysts were further investigated by XPS analysis. The overview XPS spectra of the samples **WO_3** and **WO_3-ZY** are shown in Fig. 4(a). The spectra clearly show the presence of W4d, W4f and O1s peaks and the respective oxidation states of the elements are indexed. The narrow range spectra of W4d and O1s correspond to **WO_3** and **WO_3-ZY** are shown in Fig. 4(b, c). The binding energy observed at around 247 and 530 eV in Fig. 4(b, c) ascribed to W4d and O1s of WO_3 respectively. An obvious, shift of W4d and O1s peaks in **WO_3-ZY** to higher binding energy value is observed in the spectra, which is assigned to the fact that the strong intraction between WO_3 and Zeolite-Y. The O1s peak shift from 530 eV to 538 eV is attributed to oxygen of WO_3 hydrogen bonded to the zeolite surface[28]. On the other hand, the particle size variation and lattice variation can also change the binding energy in XPS. The particle size reduction will results in higher binding energy shift, which clearly shows the reduction of WO_3 particle size in **WO_3-ZY**.[29] This reduction in particle size is good agreement with results obtained from FESEM and TEM analysis.

Raman spectral analysis

The Raman spectra of the prepared catalysts consist of three main regions such as less than 200, 200–400 and 600–900 cm^{-1} as shown in Fig. 5(a) which was well matched with the literature report of monoclinic tungsten oxide phase. [30, 31] The Raman peaks at 135 and 184 cm^{-1} are corresponds to the $(W_2O_2)_n$ chains. [30] The W–O–W bending modes of bridging oxide ion peaks are appearing at 273 and 329 cm^{-1}.[30] The peaks at 720 and 809 cm^{-1} are attributed to the W–O–W stretching mode in tungsten oxide network. [32] The intensity of the Raman peaks was very low for the catalyst **WO_3-ZY** which may be due to the very small particle size.

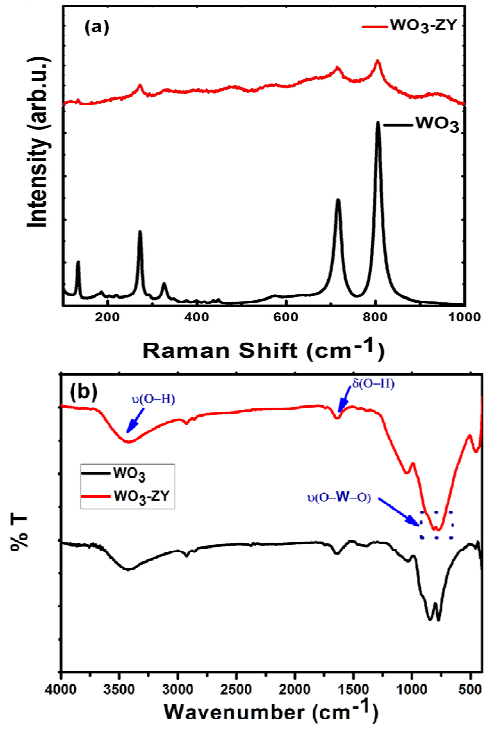

Fig.5 (a) Raman and (b) FT-IR spectrum of **WO_3** and **WO_3-ZY.**

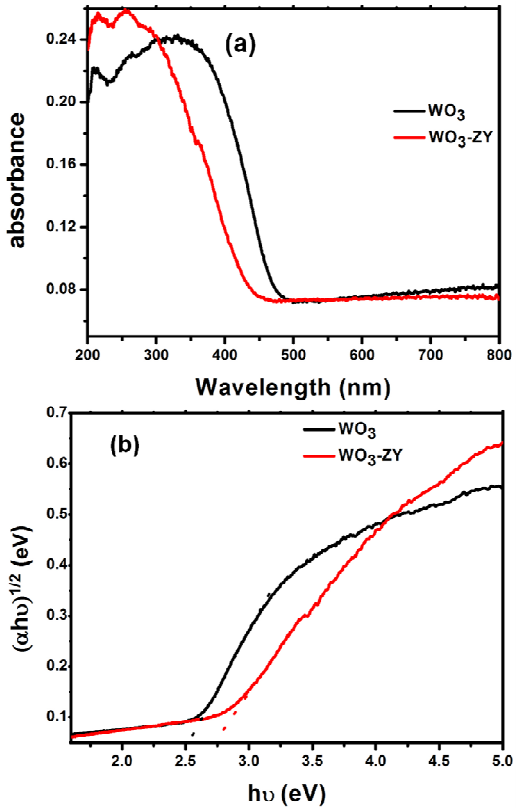

Fig.6 (a) UV-Vis DRS and (b) plot of $(\alpha h\nu)^{1/2}$ versus hν of **WO_3** and **WO_3-ZY.**

FT-IR analysis

The FT-IR spectral characterization was carried out to analyze the catalysts and the obtained spectrum is shown in Fig. 5(b). The strong absorption peaks for pure WO_3 was observed in the range of 500–900 cm^{-1} which corresponds to the ν(O–W–O) stretching mode.[33] The peak at around 750 cm^{-1} attributed to the ν(O–W–O) stretching mode.[34] The bands in the range of 3200–3550 cm^{-1} are ascribed to the ν(O–H) stretching and the band at 1625 cm^{-1} is corresponds to the δ(O–H) bending modes of the coordinated water.[33]

Optical property

The optical property of the catalysts was investigated by UV-Vis DRS spectroscopic technique and shown in Fig. 6(a). The spectrum reveals that all catalysts have absorption edges above 400 nm wavelength. The band gap energies of the samples can be calculated by the following equation.[35, 36]

$$\alpha h\nu = A(h\nu - E_g)^{n/2} \quad (1)$$

Where α, ν, E_g and A are absorption coefficient, frequency of the light, band gap energy and a constant respectively. And n is the type of optical transition of a semiconductor which is 1. The band gap energy (E_g) of the catalysts can be calculated from the intercept of the tangent to the X axis from a plot of $(\alpha h\nu)^{1/2}$ versus energy (hν) as given in Fig. 6(b). The calculated band gap energies of the samples are 2.52 and 2.73 eV for **WO_3** and **WO_3-ZY** respectively. The valance bad (VB) edge potential of a semiconductor at the point of zero charge can be calculated from the following equation.[37]

$$E_{VB} = X - E^e + 0.5E_g \quad (2)$$

Where E_{VB} is the VB edge potential, X is the electronegativity of the semiconductor, E^e is the energy of free electrons on the

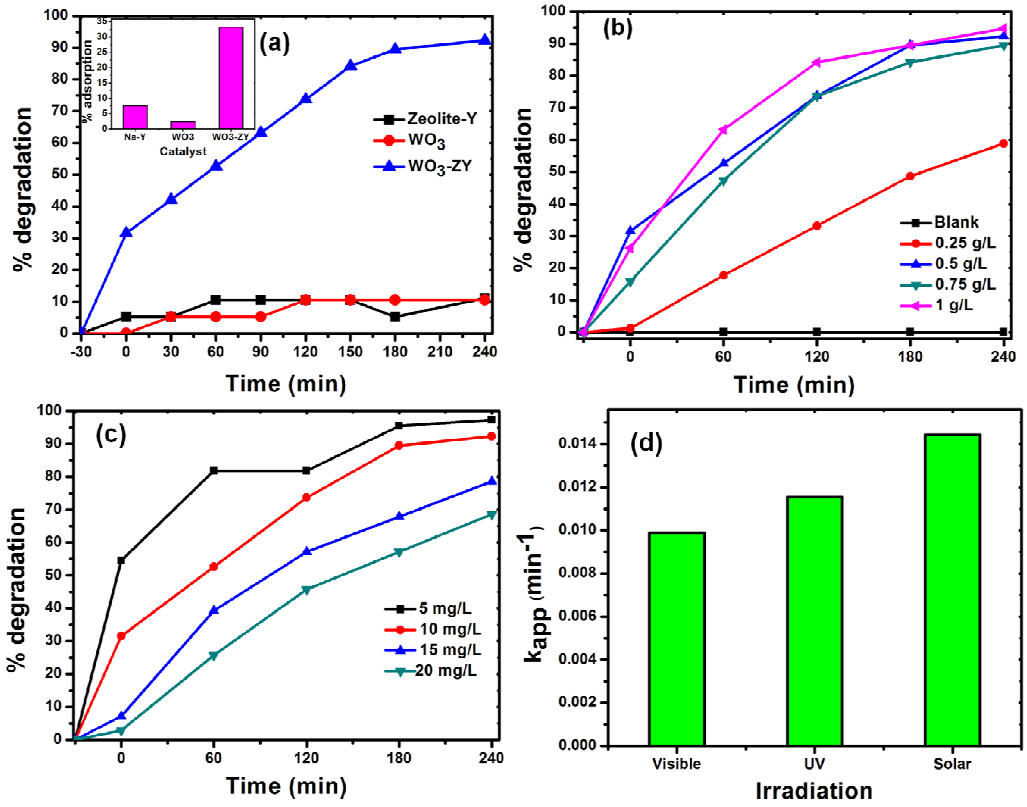

Fig.7 % degradation of RhB under visible light irradiation (a) over different catalysts, over **WO_3-ZY** (b) on varying the amount of catalyst, (c) on varying the amount of RhB and (d) under different light irradiation.

hydrogen scale (about 4.5 eV), E_g is the band gap energy of the semiconductor. The conduction band (CB) edge potential (E_{CB}) can be determined by $E_{CB} = E_{VB} - E_g$. The X value for WO_3 is ca. 6.60 and the calculated E_{VB} and E_{CB} of the catalysts are 3.36 and 0.84 eV respectively for **WO_3** and 3.46 and 0.73 eV respectively for **WO_3-ZY**. The band gap energy changes and blue shift in the UV-Vis spectrum clearly suggest that, the particle size of the catalyst is decreased.

Photocatalytic activity

The photocatalytic activity of the prepared catalysts for the degradation of RhB is demonstrated under visible, UV and solar light irradiation. Before that, the blank experiment without any catalyst was carried out to test the stability of RhB under visible, UV and solar light irradiation. The UV-vis spectral changes of RhB under various light irradiations were recorded (see Fig. S1-3 in supporting informations). There is no significant changes were observed in the UV-vis spectrum which confirms the degradation of RhB is almost zero or negligible under the various light irradiation in the absence of any catalyst. These experimental results show RhB in aqueous medium is highly stable under the given light irradiation. The % degradation of RhB was calculated by the following equation (eqn (3)).

$$\%D = (A_o - A_t)/A_o \times 100 \quad (3)$$

Where, %D is the percentage of degradation, A_o and A_t are initial absorption and absorption at time t respectively.

Photocatalytic degradation of organic compounds usually follows the pseudo-first order kinetics model. The rate constant for the degradation of RhB is calculated using the following Langmuir-Hishelwood kinetic equation.[38, 39]

$$\ln(C_0/C) = k_{app}t \quad (4)$$

Where, Co is the initial concentration of the dye solution (mol L^{-1}), C is the concentration of the dye solution at time t (mol L^{-1}), k_{app} is the apparent rate constant (min^{-1}).

The rate constant for the degradation of RhB was calculated from the slop of the plot ln(Co/C) Vs irradiation time.

Under visible light

The photocatalytic activity for the degradation of RhB by the catalysts under visible light irradiation is shown in Fig. 7(a). The enhanced photocatalytic activity was observed by the catalyst **WO_3-ZY** which may be due to high % adsorption of dye on the surface of the catalyst. The % adsorption of RhB on the surface of the catalysts under dark in 30 min is shown in the insert figure of Fig. 7(a). The high % adsorption of about 30% was achieved by the catalyst **WO_3-ZY** whereas **WO_3** shows less than 10 % of adsorption. This high % adsorption may be due to decreasing the particle size of **WO_3** on zeolite-Y which may provide more active sites to adsorb dye molecules. This study experimentally confirms the reduced particle size of the catalyst **WO_3-ZY**. For comparison, the photocatalytic degradation of RhB by Na-Y was also done and which is not active in visible light as shown in Fig. 7(a).

Optimization study

To effectively utilize the catalyst in low amount and get high efficiency at an optimum dye concentration, two sets of

experiments were done. First is changing the amount of **WO_3-ZY** from 0.25 g/L to 1 g/L keeping 10 mg/L dye concentration as constant. Second is changing the dye concentration from 5 mg/L to 20 mg/L keeping 0.5 g/L catalyst as constant. The increased % degradation of 58 % to 92 % was observed as increasing the amount of the catalyst from 0.25 g/L to 0.5 g/L respectively. This may be due to increasing the availability of active sites on the catalyst surface as increasing the catalyst amount. On further increasing the amount of catalyst, the degradation efficiency does not increase as shown in Fig. 7(b). This may be due to the aggregation of a high amount of catalyst, which causes reduced the active sites for the adsorption of dye molecules and photons. Moreover, high concentration of catalyst creates turbidity and thus reducing the penetration intensity of light radiation by scattering effect.[40, 41] As the dye concentration increases, the photocatalytic activity decreases as shown in Fig. 7(c). This may be due to decreasing the number of photons reaching on the surface of the catalyst since more photons absorption by dye molecules.[42] These experimental results suggested that the optimum reaction condition as 0.5 g/L catalyst and 10 mg/L dye concentration to achieve better efficiency.

Under UV and Solar light

The photocatalytic efficiency of the catalyst **WO_3-ZY** was investigated under UV and solar light irradiation. The photocatalytic degradation of about 86 % was observed at 140 min under UV light irradiation which is very high efficiency when compare with **WO_3** (see Fig. S4 in supporting information for the degradation profile of different catalyst), this result consistent with the one obtained under visible light irradiation. Under solar light irradiation, 95 % of degradation was observed at 180 min. The rate constant for the degradation of RhB under different light irradiation are given in Fig. 7(d). The rate constant was increases as the order of Visible<UV<Solar light irradiation. The high rate constant under solar light irradiation suggested that the catalyst can be efficiently used for the conversion of solar energy.

Reaction mechanism and degradation pathway

Recombination of electron-hole pair

The photocatalytic efficiency of a catalyst can be enhanced by inhibiting the recombination of photo generated electron-hole pair. It is well known that, the lower PL intensity of the catalyst can have a less recombination rate and high photocatalytic activity as the recombination of electron-hole pair release energy in the form of fluorescence emission. [43, 44] The PL spectra of the catalysts are shown in Fig. 8(a). The PL intensity of the catalyst **WO_3-ZY** shows lowest intensity compared with pure **WO_3**. It is suggested that **WO_3-ZY** have lowest electron-hole pair recombination rate which is consistent with the high photocatalytic activity observed. This decrease in the PL intensity may be due to the small particle size of the catalyst which can increase the surface area and thus increases the interfacial charge-carrier transfer.[19]

Role of electron acceptors

The electron acceptors like air and hydrogen peroxide can create more active radicals of $\cdot O_2^-$ and $\cdot OH$ respectively which is strong enough to degrade organic molecule. The experimental results for the photocatalytic degradation of RhB over **WO_3-ZY** in the presence of air, hydrogen peroxide (5 mmol) and no acceptor

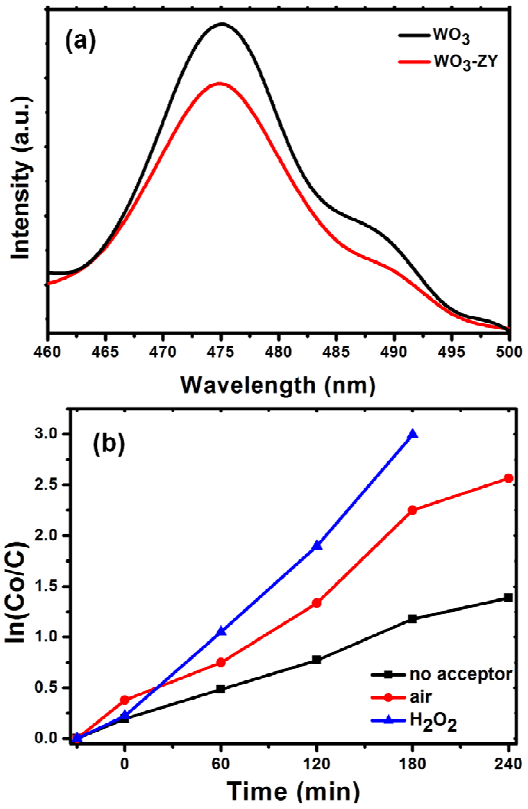

Fig.8 (a) PL spectrum of the catalysts and (b) effect of electron acceptor for the degradation of RhB

under visible light irradiation are shown in Fig. 8(b). The k_{app} of 0.0052 min^{-1} in the absence of electron acceptor was increased to 0.0143 min^{-1} by the addition of hydrogen peroxide. This enhanced photocatalytic activity in the presence of electron acceptors may be due to decreasing the recombination rate of electron-hole pairs and formation of more active radicals.

Role of active species

The holes (h^+) and radicals trapping experiments were carried out to investigate the role of reactive species in the photocatalytic degradation of RhB over **WO_3-ZY** under visible light irradiation. The changes of k_{app} for the degradation of RhB in the presence of different scavengers (5mmol) are shown in Fig. 9(a). When t-BuOH (as $\cdot OH$ scavenger) added,[45] the k_{app} was slightly decreased to 0.0035 min^{-1} from 0.0052 min^{-1}. On the other hand, the k_{app} of RhB degradation was decreased to 0.0023 min^{-1} when added with benzoquinone (BQ) as $\cdot O_2^-$ scavenger.[46, 47] However, on the addition of ammonium oxalate (AO) as h^+ scavenger,[48] the k_{app} decreased radically to 0.0005 min^{-1}. These decreases in the k_{app} on the addition of different scavengers suggested that h^+ and $\cdot O_2^-$ plays a major role, whereas $\cdot OH$ is a minor active species for the degradation of RhB. The active radical $\cdot O_2^-$ can be formed by reacting photo generated electrons react with O_2 molecules adsorbed on the surface of the catalyst[1] which indicates that the O_2 is an efficient electron acceptor to generate $\cdot O_2^-$ and inhibiting the electron-hole pair recombination.[49, 50]

Possible reaction mechanism and degradation pathway

Based on the effect of scavengers, a possible mechanism for the photocatalytic degradation of RhB over **WO_3-ZY** is illustrated in Fig. 9(b). As shown in Fig. 9(b), the electron-hole pair was created by the illumination of the catalyst. Then the photoinduced

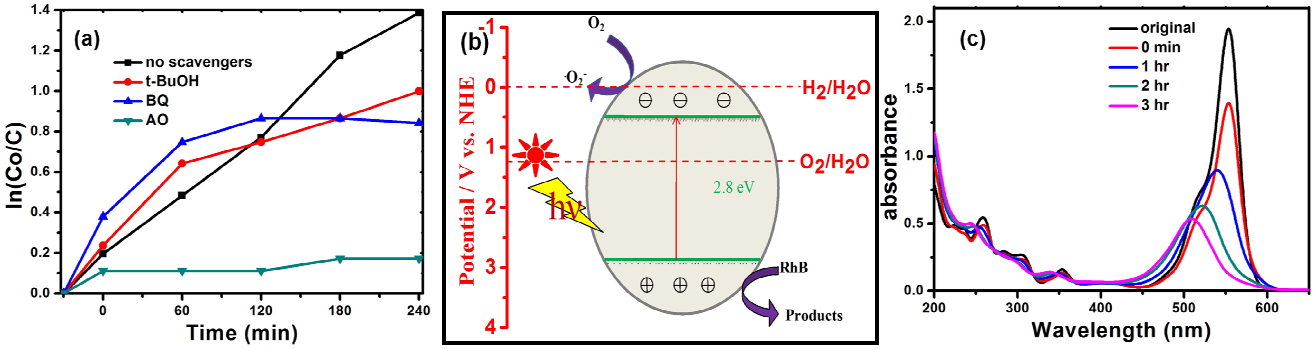

Fig.9(a) Effect of different scavengers, (b) Possible mechanism and (c) The temporal UV-vis absorption spectral variation for the photocatalytic degradation of RhB over **WO_3-ZY**.

electrons in the CB react with O_2 molecule adsorbed on the surface of the catalyst and forms $\cdot O_2^-$ radicals to degrade RhB. Meanwhile, the photoinduced holes in the VB can directly degrade RhB. The photocatalytic degradation of RhB can be illustrated as follows eqn (5-8):

$$WO_3 + h\nu \rightarrow e^-_{CB} + h^+_{VB} \quad (5)$$

$$e^-_{CB} + O_2 \rightarrow \cdot O_2^- + \text{catalyst} \quad (6)$$

$$RhB + \cdot O_2^- \rightarrow \text{products} \quad (7)$$

$$RhB + h^+_{VB} \rightarrow \text{products} \quad (8)$$

It is well known that the degradation of RhB proceeds via two processes of N-de-ethylation and destruction of conjugated structure.[51] The temporal UV-vis absorption spectral variation for the photocatalytic degradation of RhB under solar light irradiation is shown in Fig. 9(c). The absorption band at 554 nm is decreased which suggest the degradation of the xanthene ring in RhB. The blue shift in the absorption spectrum ascribed the formation of de-ethylated RhB.[52] Based on the results obtained from the UV-vis spectral changes, we proposed the degradation pathway of RhB schematically. As shown in Scheme 1, the degradation of RhB occurred through de-ethlyation process then the destruction of conjugated xanthane structure in RhB which gives the benzenoid intermediates.[53] After that, the ring opening of the intermediates and mineralization process was demonstrated.

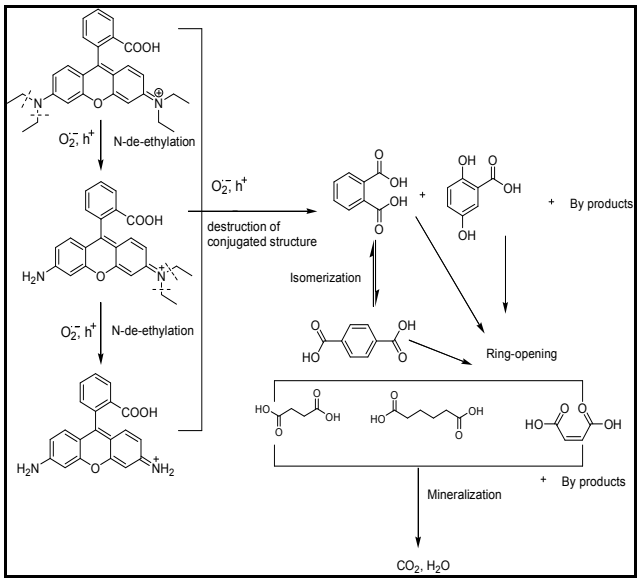

Scheme 1 Proposed degradation pathway for the photocatalytic degradation of RhB.

Conclusion

In this study, we have successfully synthesized the pure WO_3 and WO_3 supported on Zeolite-Y and well characterized. The TEM, FESEM and adsorption study confirms that, the catalyst **WO_3-ZY** have very small particle size of 8 nm. The photocatalytic activity of the prepared catalysts was investigated for the degradation of RhB under visible, UV and solar light irradiation. The enhanced photocatalytic activity was observed by the catalyst **WO_3-ZY**. The higher photocatalytic activity of **WO_3-ZY** under solar light irradiation compared to other light irradiation suggests the catalyst can be utilized for solar energy conversion. The efficient electron-hole pair separation of the catalyst is benefited to obtain enhanced photocatalytic activity which was confirmed by PL spectra. The effect of scavengers test shows active species h^+ and $\cdot O_2^-$ play a major role in the photocatalytic degradation of RhB. The proposed mechanism for the photocatalysis and degradation pathway of RhB was illustrated, which involves N-de-ethylation, destruction of conjugated structure, ring opening and mineralization process.

ACKNOWLEDGEMENT

The authors thank to DST-SERC for financial support, sanction no. SR\FT\CS-042\2008.

Notes and references

[a] *Department of Chemistry, Anna University, BIT campus, Tiruchirappalli-620 024, Tamil Nadu, India; E-mail: jothivenkat@yahoo.com*

[b] *Centre for Nanoscience and Nanotechnology, School of Physics, Bharathidasan University, Tiruchirappalli-620 024, Tamil Nadu, India.*

† Electronic Supplementary Information (ESI) available: PXRD spectrum of Zeolite-Y, UV-Vis. Spectral changes of RhB under visible, UV and solar light irradiation without any catalyst and % degradation of RhB under UV light irradiation by different catalyst. See DOI: 10.1039/b000000x/

1 M. R. Hoffmann, S.T. Martin, W. Choi, D.W. Bahnemann, Chem. Rev., 1995, **95**, 69.

2 S. C. Zhang, J. D. Shen, H. B. Fu, W. Y. Dong, Z. J. Zheng, L. Y. Shi, J. Solid State Chem., 2007, **180**, 1456.

3 A. Fujishima, K. Honda, Nature, 1972, **238**, 37.

4 W. K. Ho, J. C. Yu, S. C. Lee, Chem. Commun., 2006, **111**, 1115.

5 Y. Cong, J. L. Zhang, F. Chen, M. Anpo, J. Phys. Chem. C, 2007, **111**, 6976.
6 H. Irie, Y. Watanabe, K. Hashimoto, J. Phys. Chem. B, 2003, **107**, 5483.
7 G. R. Bamwenda, H. Arakawa, Appl. Catal. A, 2001, **210**, 181.
8 Z. G. Zhao, M. Miyauchi, Angew. Chem. Int. Ed., 2008, **47**, 7051.
9 D. Chen, J. H. Ye, Adv. Funct. Mater., 2008, **18**, 1922.
10 Y. F. Guo, X. Quan, N. Lu, H.M. Zhao, S. Chen, Environ. Sci. Technol., 2007, **41**, 4422.
11 Z. G. Zhao, M. Miyauchi, J. Phys. Chem. C, 2009, **113**, 6539.
12 K. Z. Lv, J. Li, X. X. Qing, W. Z. Li, Q. Y. Chen, J. Hazard. Mater., 2011, **189**, 329.
13 J. Papp, S. Soled, K. Dwight, A. Wold, Chem. Mater., 1994, **6**, 496.
14 H. W. Choi, E. J. Kim, S. H. Hahn, Chem. Eng. J., 2010, **161**, 285.
15 S. M. Sun, W. Z. Wang, S. Z. Zeng, M. Shang, L. Zhang, J. Hazard. Mater., 2010, **178**, 427.
16 D. Su, J. Y. Wang, Y. P. Tang, C. Liu, L. F. Liu, X. J. Han, Chem. Commun., 2011, **47**, 4231.
17 J. Kim, C. W. Lee, W. Choi, Environ. Sci. Technol., 2010, **44**, 6849.
18 X. F. Cheng, W. H. Leng, D. P. Liu, J. Q. Zhang, C. N. Cao, Chemosphere, 2007, **68**, 1976.
19 A. Purwanto, H. Widiyandari, T. Ogi, K. Okuyama, Catal. Commun., 2011, **12**, 525.
20 W. Zhang, K. Wang, Y. Yu, H. He, Chem. Eng. J., 2010, **163**, 62.
21 A. Nezamzadeh-Ejhieh, Z. Salimi, Desalination, 2011, **280**, 281.
22 Z. M. El-Bahy, M. M .Mohamed, F. I. Zidan, M. S. Thabet, J. Hazard. Mater., 2008, **153**, 364.
23 A. Nezamzadeh–Ejhieh, Z. Banan, Desalination, 2011, **279**, 146.
24 H. Chen, A. Matsumoto, N. Nishimiya, K. Tsutsumi, Colloids Surf. A., 1999, **157**, 295.
25 M. Alvaro, E. Carbonell, M. Espla, H. Garcia, Appl. Catal. B: Environ., 2005, **57**, 37.
26 M. Aleksic, H. Kusic, N. Koprivanac, D. Leszczynska, A.L. Bozic, Desalination, 2010, **257**, 22.
27 S. Supothina, P. Seeharaj, S. Yoriya, M. Sriyudthsak, Ceram. Int., 2007, **33**, 931.
28 I. Gouzman, M. Dubey, M. D. Carolus, J. Schwartz, S. L. Bernasek, Surface Science, 2006, **600**, 773.
29 B. Richter, H. Kuhlenbeck, H. J. Freund, P. S. Bagus, Phys. Rev. Lett.2004, **93**, 26805.
30 B. Pecquenard, H. Lecacheaux, L. Livage, C. Julien, J. Solid State Chem., 1998, **135**, 159.
31 M. Boulova and G. Lucazeau, J. Solid State Chem., 2002, **167**, 425.
32 H. Habazaki, Y. Hayashi and H. Konno, Electrochim. Acta, 2002, **47**, 4181.
33 H. I. S. Nogueira, A. M. V. Cavaleiro, J. Rocha, T. Trindade, J. D. P. D. Jesus, Mater. Res. Bull., 2004, **39**, 683.
34 C. Guery, C. Choquet, F. Dujeancourt, J. M. Tarascon, J. C. Lassegues, J. Solid State Electrochem., 1997, **1**, 199.
35 M. A. Butler, J. Appl. Phys., 1977, **48**, 1914.
36 J. Zeng, H. Wang, Y. C. Zhang, M. K. Zhu, H. Yang, J. Phys. Chem. C, 2007, **111**, 11879.
37 X. Zhang, L. Z. Zhang, T. F. Xie, D. J. Wang, J. Phys. Chem. C, 2009, **113**, 7371.
38 J. G. Yu, H .G. Yu, B. Cheng, X. J. Zhao, J. C. Yu, W. K. Ho, J. Phys. Chem. B, 2003, **107**, 13871.
39 H. Kumazawa, M. Inoue, T. Kasuya, Ind. End. Chem. Res., 2003, **42**, 3237.
40 A. Akyol, H. C. Yatmaz, M. Bayramoglu, Appl. Catal. B: Environ., 2004, **54**, 19.
41 B. Neppolian, H. C. Choi, S. Sakthivel, B. Arabindoo, V. Murugesan, Chemosphere, 2002, **46**, 1173.
42 M. A. Rauf, S. S. Ashraf, Chem. Eng. J., 2009, **151**, 10.
43 T. J. Cai, M. Yue, X. W. Wang, Q. Deng, Chin. J. Catal., 2007, **28**, 10.
44 H. Tang, K. Prasad, R. Sanjines, P. E. Schmid, F. Levy, J. Appl. Phys., 1994, **75**, 2042.
45 T. Xu, L. Zhang, H. Cheng, Y. Zhu, Applied Catalysis B: Environmental, 2011, **101**, 382.
46 J. Bandara, J. Kiwi, New J. Chem., 1999, 23, 717.
47 M. C. Yin, Z. S. Li, J. H. Kou, Z. G. Zou, Environ. Sci. Technol., 2009, **43**, 8361.
48 N. Zhang, S. Q. Liu, X. Z. Fu, Y. J. Xu, J. Phys. Chem. C, 2011, **115**, 9136.
49 Y. Y. Li, J. S. Wang, H. C. Yao, L. Y. Dang, Z. J. Li, J. Mol. Catal. A: Chem., 2011, **334**, 116.
50 Y. Q. Yang, G. K. Zhang, S. J. Yu, X. Shen, Chem. Eng. J., 2010, **162**, 171.
51 C. Chen, X. Li, W. Ma, J. Zhao, H. Hidaka, N. Serpone, J. Phys. Chem. B, 2002, **106**, 318.
52 N. Bao, X. Feng, Z. Yang, L. Shen, X. Lu, Environ. Sci. Technol., 2004, **38**, 2729.
53 Z. He, C. Sun, S. Yang, Y. Ding, H. He, Z. Wang, J. Hazard. Mater., 2009, **162**, 1477.